

Investigating the importance of social vulnerability in opioid-related mortality across the United States

Andrew Deas^{1,*}, Adam Spannaus², Dakotah D. Maguire², Jodie Trafton³, Anuj J. Kapadia², and Vasileios Maroulas^{1,*}

Author Affiliations:

¹Department of Mathematics, University of Tennessee, Circle Dr, Knoxville, 37916, TN, USA

²Computational Sciences and Engineering Division, Oak Ridge National Laboratory, Bethel Valley Road, Oak Ridge, 37830, TN, USA

³Office of Mental Health and Suicide Prevention, Veterans Health Administration, Willow Road, Palo Alto, 94025, CA, USA

*Corresponding authors:

Andrew Deas

1414 Cumberland Ave, Knoxville, TN 37996

adeas1@vols.utk.edu

Vasileios Maroulas

Ayres Hall, 1403 Circle Dr, Knoxville, TN 37916

vmaroula@utk.edu

Classification: Research Report

Keywords: opioid crisis, anomaly analysis, machine learning, XGBoost, autoencoder

Included in this pdf file: main text, figures 1 through 8, tables 1 and 2

Abstract

The opioid crisis remains a critical public health challenge in the United States. Despite national efforts which reduced opioid prescribing rates by nearly 45% between 2011 and 2021, opioid overdose deaths more than tripled during this same period. Such alarming trends raise important questions about what underlying social factors may be driving opioid misuse. Using county-level data across the United States, this study begins with a preliminary data analysis of how the rates of thirteen social vulnerability index variables manifest in counties with both anomalously high and low mortality rates, identifying patterns that warrant further investigation. Building on these findings, we further investigate the importance of the thirteen SVI variables within a machine learning framework by employing two predictive models: XGBoost and an autoencoder. Both models take the thirteen SVI variables as input and predict county-level opioid-related mortality rates. This allows us to leverage two distinct feature importance metrics: information gain for XGBoost and a Shapley gradient explainer for the autoencoder. These metrics offer two unique insights into the most important SVI factors in relation to opioid-related mortality. By identifying the variables which consistently rank as most important, this study highlights key social vulnerability factors that may play critical roles in the opioid crisis.

Significance Statement:

The opioid crisis has increasingly shifted from prescription opioids to illegal drugs like heroin and fentanyl. This shift has resulted in surging opioid-related mortality rates and greater involvement with the criminal justice system. Despite this increased risk of severe legal consequences, individuals continue to seek opioids in large numbers, driven at least in part by socioeconomic factors. This study investigates the importance of thirteen social vulnerability factors that may be influencing this behavior. By identifying the factors which consistently rank as most important, this research points to key targets for public health interventions focused on reducing opioid-related mortality and fostering long-term recovery in the nation's most vulnerable regions.

Introduction

The opioid crisis in the United States remains one of the most daunting and complex public health challenges in recent history. Although initially driven by prescription practices, national efforts and legislation have significantly reduced opioid prescriptions from 257.9 million in 2011 to 143.4 million in 2020, a 44.4 percent decrease [1–3]. This decline in prescriptions has not led to a corresponding reduction in opioid-related overdose deaths. On the contrary, opioid overdose death rates have surged [4]. In 2011, the rate stood at 7.3 per 100,000 persons, but by 2021, it had more than tripled to 24.7 per 100,000 persons [5].

These unsettling trends highlight the opioid epidemic’s evolving shift from prescription opioids to illegal drugs such as heroin and fentanyl [6]. As the crisis increasingly revolves around illicit opioids, more individuals with opioid use disorder (OUD) are coming into contact with the criminal justice system [6]. Yet despite this increased risk of legal action, individuals continue to seek access to opioids at alarming rates; this raises important questions about what underlying factors may be driving this behavior. Among these factors, components of the social vulnerability index (SVI)—a compound measure of a population’s susceptibility to external stresses on human health—have been shown to play a crucial role in the opioid crisis [7–9]. For example, social vulnerability factors have been identified as reliable predictors of opioid-related mortality [10], counties with higher social vulnerability rates tend to exhibit higher rates of OUD [11], and communities with greater vulnerability due to housing type and lack of transportation have reduced access to medications for OUD [9].

Using county-level data from 2010 to 2022, this study investigates the importance of thirteen SVI variables in relationship to opioid-related mortality. Included in this analysis are the variables: below poverty, unemployment, no high school diploma, aged 65 and older, aged 17 and younger, single-parent households, limited English ability, minority status, multi-unit structures, mobile homes, crowding, no vehicle, and group quarters. A detailed definition of each feature is provided in table 1.

The mortality rates were sourced from the Center for Disease Control and Prevention’s Wide-ranging ONline Data for Epidemiologic Research (CDC WONDER) system [12]. The CDC WONDER database, while invaluable for mortality data, suppresses death counts in counties with fewer than 10 deaths. As a result, mortality rates were missing for nearly half of the nation’s counties in each year of the study period. To meaningfully use this data, we developed a robust methodology to impute the missing values from neighboring counties.

Using this data, our study begins with a preliminary analysis of how each SVI variable’s rates manifest in counties exhibiting both anomalously high and low mortality rates. Anomalies are identified by fitting a lognormal distribution to the nonzero mortality rates for each year; anomalously

high rates are then defined as those above the 98th percentile of the annual fitted distribution and anomalously low rates as those below the 2nd percentile. By identifying counties with exceedingly high mortality rates, we seek to gain an understanding of which SVI factors might be linked to particularly severe opioid-related outcomes. Likewise, by identifying counties with exceptionally low mortality rates, we explore which SVI features may help to mitigate the crisis by possibly playing a role in the minimal mortality rates seen in these areas. Of particular interest are variables that exhibit influence at both ends of the mortality spectrum—those that show their highest rates in counties with extremely high mortality and their lowest rates in counties with extremely low mortality. Variables exhibiting this duality may play particularly critical roles in the crisis, as their influence on both ends of the mortality spectrum suggest that lowering rates of these variables could lead to measurable reductions in opioid-related mortality.

The first step in our analysis provides a data-driven foundation for the machine learning models that follow; these initial insights are further investigated within a predictive framework. The secondary phase of the study employs two models: 1) XGBoost, a decision tree-based approach, and 2) a modified autoencoder, a neural network model. In both models, the thirteen SVI variables serve as input, and the output is a single vector consisting of opioid-related mortality rate predictions for each county in the nation. This approach allows us to leverage two distinct feature importance metrics (each inherent to its respective model), providing two unique perspectives on which factors may be most important in predicting opioid-related mortality. By utilizing both models, we mitigate the risks of relying only on a single model’s interpretation, ensuring a more comprehensive examination of the most important SVI factors in opioid-related mortality.

The first machine learning model employed in this study is XGBoost; a powerful decision tree-based model with a strong track record in classification and regression tasks across various domains [13–16]. In this study, XGBoost is used to predict yearly opioid-related mortality rates based on the previous year’s SVI data. Although lagging the input variables introduces some temporal structure, XGBoost is inherently limited in modeling time dependencies. It treats each year’s data independently and lacks the memory mechanisms present in more advanced models. However, XGBoost has a built-in and highly effective mechanism for evaluating feature importance. It utilizes information gain to quantify how much each feature improves predictive accuracy when splitting a node in a decision tree. Consequently, the most important features in the XGBoost model are those that most improve its mortality rate predictions.

The second machine learning model utilized in this study is a modified autoencoder. Autoencoder models consist of two main parts: an encoder and a decoder [17–19]. The encoder compresses input data into a compact, lower-dimensional latent space, generating representations called encodings. The decoder then projects these encodings back into the original data space. This process enables the model to learn essential features in the data by minimizing a loss between the target

and the decoder’s output. In this study, we modify the general autoencoder structure with an initial convolutional layer that aggregates the thirteen SVI variables used as input. This input is lagged by one year, and the corresponding output is a vector of yearly mortality rate predictions for each county in the nation.

While the autoencoder can learn temporal patterns in the data through training, it lacks a built-in feature importance mechanism. To address this, we applied a Shapley Gradient Explainer to the initial convolutional layer [20]. This method generates estimates, called SHAP values [21], that quantify each feature’s impact on mortality rate predictions by measuring the autoencoder’s sensitivity to small changes in that feature. Thus, the most important features in the autoencoder model are those for which minor perturbations produce the greatest effects on predictions.

Leading off with a preliminary data analysis and following up with two predictive machine learning models, this study provides a thorough investigation into the importance of thirteen SVI variables in relation to opioid-related mortality. In doing so, we aim to shed light on key social factors that may be exacerbating the opioid epidemic and driving individuals to seek access to opioids. Ultimately, this study offers valuable insights for shaping future public health interventions and strategies aimed at addressing the ongoing opioid crisis.

Results

Anomaly analysis

This study begins by with a preliminary investigation into how the rates of each SVI variable manifest in counties exhibiting both anomalously high and low mortality rates. These anomalies are categorized into two groups: counties with exceedingly high mortality rates, termed ‘hot anomalies,’ and counties with exceptionally low mortality rates, termed ‘cold anomalies.’ To define the thresholds categorizing these anomalies, we fit a distribution to each year of mortality data. In any given year, a significant portion of the imputed mortality data consists of zero values, at most 947 counties, or 30.12% of the data. For this reason, zero values do not represent anomalous cases and were therefore excluded. As a result, the set of possible fitted distributions was restricted to those defined over the range $(0, \infty)$.

To determine the best-fitting distribution, we tested several candidates, including Gamma, Weibull, and lognormal distributions. Each year, the lognormal distribution provided the best visual fit. Using these fitted lognormal distributions, anomalies are defined annually as follows: Hot anomalies are counties with nonzero rates above the 98th percentile of the yearly fitted distribution, while cold anomalies are those whose nonzero rates fall below the 2nd percentile. To select the size of these tails, we assessed 1%, 2%, and 3% thresholds. In some years, a 1% tail produced no cold anomalies, whereas the 2% tail always provided them. While a 3% tail also could have been used,

to maximize the anomalous nature of the rates, we opted for the tightest bounds that still yielded cold anomalies for analysis each year. Figure 1 shows how the anomalies in 2016 change with 1%, 2%, and 3% tails.

To visualize the distribution of each SVI variable’s rates across the nation, we construct yearly boxplots that illustrate the variation in rates among hot, cold, and non-anomalous counties. The boxplots for 2010, 2016 and 2022 are shown in figure 2. These visualizations provide a detailed view of the variability and spread of each variable in the different county categories. To complement this, we summarize the boxplots by ranking the features according to their average mean rates, from highest to lowest in the hot counties and from lowest to highest in the cold counties. These summaries are presented in figure 3, where each feature’s yearly mean rates are shown using colored bars, while the black bars display each feature’s average mean rate across all years in the study.

Figure 3a summarizes the boxplot results for the hot anomalies. Among these hot counties, the variable with the highest average mean rate is no vehicle (75.40), followed by below poverty (75.22), no high school diploma (73.48), unemployment (70.18), and mobile homes (68.61). The high ranking of these variables means they tend to manifest their highest rates in counties with anomalously high opioid-related mortality. This suggests that opioid-related mortality may be exacerbated by elevated levels of these factors. Beyond these top five, rates noticeably decline, starting with single-parent households (54.61) and continuing to drop further down the list. At the bottom are limited English ability and minority status, meaning they have the lowest average rates in the hot counties. This suggests that these factors may contribute the least to the exceptionally high mortality rates observed in the hot counties.

Figure 3b summarizes the boxplot results for the cold anomalies. Among these cold counties, the variable with the lowest average mean rate is unemployment (35.58), followed by multi-unit structures (39.66), single-parent households (39.89), limited English ability (42.22), and no vehicle (42.84). The high ranking of these variables means they tend to manifest their lowest rates in counties with anomalously low opioid-related mortality. This suggests that opioid-related mortality may be alleviated by lower levels of these factors. Beyond these top five, mean rates only gradually increase, except at the bottom, where a significant jump is observed for the variable aged 65 or older. This factor stands out with the highest average mean rate (61.74) in the cold anomalies, indicating that counties with anomalously low opioid-related mortality tend to have a significantly higher population of persons aged 65 or older.

Notably, only two variables—unemployment and no vehicle—manifested both their highest rates in counties with anomalously high mortality and their lowest rates in counties with anomalously low mortality. This duality suggests that these variables may play a particularly significant role at both extreme ends of the mortality rate spectrum: High levels of these variables may contribute to increased opioid-related mortality, whereas low levels may play a role in reducing it. These

preliminary insights lay the data-driven foundation for the subsequent machine learning analysis by highlighting key patterns that warrant further investigation.

Efficacy of machine learning models

The efficacy of both machine learning models in forecasting county-level mortality rates is evaluated using accuracy and error metrics. For each county, the error is measured as the absolute residual. To assess overall accuracy, the maximum absolute residual—indicating the largest annual prediction error—is used as a benchmark: each county’s error is normalized by this highest observed error across the country. The efficacy of the models is summarized in table 2, which presents the average errors, maximum errors, and average accuracy of both models for each predictive year in the study period. Additionally, fig. 4 and fig. 5 provide visual representations of the 2022 efficacy results via error histograms and accuracy maps.

Notably, both models show a significant increase in average and maximum errors beginning in 2020 which persists through 2022. Some of these errors are attributable to problems inherent in data suppression. For instance, the maximum error for both models in 2022 stems from Menominee County, Wisconsin, where the 2021 mortality rate was suppressed and imputed from neighboring counties as 26.16. Yet in 2022, this county had a reported rate of 238.27—an extreme increase from the previous year that neither model could predict. However, not all large errors are due to data suppression. For example, the second largest error in 2022 for both models occurs in Bath County, Kentucky. This county reported mortality rates of 86.09 in 2021 and 163.69 in 2022. These outliers are highlighted in fig. 4, which displays the complete 2022 error distributions for both models, providing a visual comparison of their error ranges.

In general, both models maintain high accuracy throughout the entire study period. While each year is treated as an independent test year by XGBoost, 2022 is the only testing year for the autoencoder. We therefore choose to present the 2022 accuracy maps for both models in fig. 5. In this image, both accuracy maps are characterized predominantly by green hues, indicating high predictive accuracy across the nation. Notably, Menominee County, Wisconsin, which had the largest 2022 error for both models, is marked correspondingly in the darkest shade of red. While Bath County, Kentucky, appears in orange on the autoencoder’s accuracy map and in yellow on XGBoost’s map. This discrepancy is due to the sharp increase in mortality rates in Bath County from 2021 to 2022, which contributed to a larger error for the autoencoder than XGBoost in that year.

XGBoost feature importance

We used XGBoost to predict opioid-related mortality rates from 2011 to 2022 based on the previous year’s SVI data. To assess each SVI feature’s importance, XGboost utilizes information

gain. This metric, eq. (1) in the materials and methods section, quantifies the improvement in the model’s predictive performance when a feature is used to split a node in a decision tree. As a result, the features with the highest gain scores are those that most significantly improve the model’s ability to predict opioid-related mortality rates.

The feature importance results for XGBoost are displayed in fig. 6a. In this image, each feature’s yearly importance scores are shown with colored bars, while each feature’s average importance score across the entire study period is represented by the black bars. These black bars rank the features from highest average importance down to lowest.

Significantly surpassing all others, unemployment (0.1585) has the highest average importance score. This is followed by minority status (0.0814), but its average importance score is only slightly over half the importance of unemployment. While its yearly importance scores fluctuate slightly, unemployment occupies the top spot every year. As we move further down the list, feature importance scores only continue to decrease. This highlights the dominant role that unemployment plays in predicting opioid-related mortality rates for XGBoost.

Autoencoder feature importance

In this study, the autoencoder model was used to predict opioid-related mortality rates from 2011 to 2022 based on the previous year’s SVI data. To determine which SVI features were most important in the autoencoder’s predictions, we applied a Shapley Gradient Explainer to the initial convolutional layer. The Shapley Gradient Explainer generates SHAP values to quantify how sensitive the autoencoder’s mortality predictions are to small changes in each feature. As a result, the most important features in the autoencoder model are those for which minor changes lead to the greatest impact on predictions.

The feature importance results for the autoencoder are showcased in Figure 6b. In this image, each feature’s yearly SHAP value is shown with colored bars, while each feature’s average SHAP value across the entire study period is represented by the black bars. These black bars rank the features from highest average importance down to lowest.

A distinct characteristic of the Shapley importance plot is the sharp increase in SHAP values across all variables in 2022. This spike is due to the fact that 2022 was the testing year for the autoencoder, meaning the model was evaluated on unseen data. Consequently, the prediction errors in 2022 were larger than in the training years. Since the Shapley gradient explainer uses these predictions to produce SHAP values, this resulted in elevated importance scores for the year 2022.

Another noteworthy aspect of the Shapley feature importance plot is the relatively low magnitude of the SHAP values overall. This is most likely a reflection of the way the autoencoder model distributes its learning across a broad range of SVI factors rather than over-relying on a few

dominant features. Nonetheless, these values still provide key insights into the relative importance of each feature to the autoencoder model.

The feature with the highest average SHAP value is crowding (0.00143), followed closely by no vehicle (0.00137) and multi-unit structures (0.00136). In fourth place is aged 65 or older (0.00131), from which SHAP values gradually decrease down to unemployment (0.00116) in seventh place. Beyond unemployment, there is a noticeable drop in the SHAP values for mobile homes and minority status. After which, there is another steep decline in importance moving down to the the last four features. This reflects the much smaller contribution these four features make to the model’s predictions.

Discussion

This study analyzed the importance of thirteen SVI variables in relation to opioid-related mortality. Our initial investigation looked at how the rates of each variable manifested in counties with anomalous mortality. Notably only two variables—unemployment and lack of vehicle access—exhibited both their highest rates in counties with anomalously high mortality and their lowest rates in counties with anomalously low mortality. This pattern suggests that high levels of these variables may contribute to increased opioid-related mortality, while lower levels may help reduce it. This means that reducing unemployment and improving vehicle access could lead to measurable reductions in opioid-related mortality, particularly in the most severely affected regions.

These preliminary insights laid the foundation for the subsequent machine learning analysis that further investigated the relationship between the SVI variables and opioid-related mortality within a predictive framework. In this analysis, we employed two machine learning models: XGBoost and an autoencoder. Feature importance was assessed using information gain for XGBoost and a Shapley gradient explainer for the autoencoder. While the feature importance rankings differed between the two models, this difference highlights the value of employing multiple approaches, as it revealed key features that might have been overlooked if only one model had been used.

In the XGBoost model, unemployment emerged as the most important feature (0.1585) by a significant margin; the second-ranked feature, minority status (0.0814), had an importance score just over half that of unemployment. This indicates that unemployment is nearly twice as strong a predictor of opioid-related mortality than any other variable in the XGBoost model. Although crowding ranked highest (0.00143) in the Shapley analysis of the autoencoder, lack of vehicle access followed closely in second place with a nearly identical importance score (0.00137). These results from the machine learning analysis align with the preliminary insights from the anomaly investigation. This alignment reinforces unemployment and lack of vehicle access as potentially key factors in opioid-related mortality.

The connection between unemployment and opioid-related outcomes is well-established [22–24]. Previous work has shown that unemployment, along with the accompanying economic hardships, significantly contributes to opioid misuse in the United States [25–27]. These studies emphasize the importance of employment-related factors in addressing the opioid crisis, and call for substance abuse treatment to remain a priority even during economic downturns. Beyond economic strain, unemployment has been shown to disrupt the structure, routine, social connections, and sense of identity that are critical to recovery for individuals with OUD [28].

Although transportation barriers have been recognized as significant obstacles to general health-care access in prior research [29–32], their impact on the opioid crisis specifically has been largely underexplored. Transportation barriers can lead to missed or delayed healthcare appointments, increased health expenditures, and poorer health outcomes [30, 33]. These issues are particularly significant in the daily life of individuals struggling with OUD. In opioid-related emergencies, such as overdoses, access to transportation becomes vital, as the lack of it can delay life-saving care. Additionally, many underserved communities facing opioid challenges often lack adequate transportation, forcing individuals without vehicles to rely on limited local resources [29, 34]. For example, research has documented an alarming rise in opioid-related overdose deaths within Black urban populations, partly attributing this trend to the lack of available transportation in these communities [35].

In addition to highlighting the importance of unemployment and lack of vehicle access in opioid-related mortality, this study also underscores the detrimental impact of the COVID-19 pandemic on the national opioid crisis. While this impact has been previously discussed [36–38], our work adds to the conversation by providing novel support. This is seen in the performance of our models, where we observe a significant increase in errors beginning in 2020 which persists through 2022. This trend is particularly notable because the autoencoder retains learned temporal patterns, whereas XGBoost treats each year of data independently without learning across time. The fact that both models exhibit similar error patterns during this period suggests that the opioid crisis worsened during the pandemic to such a degree that previous data patterns no longer provided useful predictive insights.

The detrimental effects of the COVID-19 pandemic on the national opioid crisis were driven in part by two key factors: social isolation and unemployment [39–41]. Unemployment in the United States surged to unprecedented levels during the pandemic, peaking at 14.8% in April 2020 and gradually declining to 6.2% in February 2021, still well above the pre-pandemic rate of 3.6% in 2019 [42]. Additionally, the social isolation caused by pandemic lockdowns was shown to have harmful effects on mental health and substance use outcomes [41]. This social isolation, experienced widely during the pandemic, mirrors the regular ongoing isolation faced by individuals without access to reliable transportation. In this way, the COVID-19 pandemic highlights the destructive impact that both unemployment and lack of vehicle access can have on the national opioid crisis.

To mitigate the impact of these variables, public health interventions could prioritize strategies

that address both economic stability and transportation access. Workforce development programs that focus on providing stable, meaningful employment opportunities could play a critical role in reducing the socioeconomic stressors that contribute to opioid misuse, particularly in regions with high opioid-related mortality. Additionally, policies aimed at improving access to affordable public transportation, especially in underserved communities, could significantly reduce the transportation barriers faced by those without access to a personal vehicle. By addressing these fundamental social vulnerabilities, targeted interventions could help reduce the impact of these two critical factors and may even promote long-term recovery in the nation’s most vulnerable areas.

This study has important limitations to note, particularly the issue of missing mortality data in the CDC WONDER dataset. Although we employed methods to address this, no approach can fully overcome the challenges posed by suppressed data. This limitation was sometimes evident when real data, missing in the previous year, became available the following year at a much higher rate than the previously imputed value. This sharp increase sometimes led to large predictive errors in both models. Future research could apply the methodologies outlined in this study to a dataset with fewer missing values, if such data is available.

Additionally, the opioid crisis is a highly complex issue, influenced by many factors beyond those considered in this study. Future work could expand on the methodologies used here by investigating a broader range of factors contributing to opioid-related mortality. Lastly, we prioritized feature importance metrics over predictive accuracy within the machine learning models. For instance, we did not perform cross-validation on the autoencoder’s input data, opting instead to preserve the natural temporal trajectory of the opioid crisis. Future research could explore cross-validation or other techniques to optimize the autoencoder’s predictive power and examine how the most important features shift when predictive accuracy is emphasized.

Materials and Methods

Mortality data

This study utilizes county-level opioid-related mortality rates, measured per 100,000 persons, from 2010 to 2022. Throughout the study period, the county structure of the United States changed due to the formation of new counties and the reconfiguration of existing ones [43]. For example, Connecticut completely restructured its county boundaries in 2022 [44]. Such changes impacted data consistency across years. Additionally, the machine learning models used in this study require a fixed state space; therefore, the data has been curated to reflect the 2022 county structure, which includes 3,144 counties. This step ensures that we provide the most up-to-date and cohesive representation of the national county landscape with respect to the data.

The mortality data were sourced from the CDC WONDER online database. The data were

pulled using underlying cause-of-death codes from the Tenth Revision of ICD (ICD-10): X40–X44 (unintentional), X60–X64 (suicide), X85 (homicide), and Y10–Y14 (undetermined) [45, 46]. It is therefore important to note that these rates serve as indicators of opioid misuse rather than exact counts of opioid overdose mortality. These data were retrieved at the county level, with the specified ICD-10 codes, while the other categories were left in their default settings.

Method for handling missing data

The CDC WONDER database suppresses death counts in counties with fewer than 10 deaths. As a result, many mortality rates were missing, about half the nation’s counties in each year of the study period. To meaningfully use this data, it was essential to develop a robust methodology for imputing the missing values. One approach used in a previous study involved imputing missing death rates utilizing available data from neighboring counties [47]. In their method, each county’s neighborhood was defined as the entire state in which that county resides. In this study, we adopt a similar approach but use a more localized strategy: we impute missing mortality rates by averaging the available rates from a county’s queen adjacent neighbors—counties that share a direct border or a corner.

Utilizing the queen adjacent neighborhoods, our methodology proceeds in a step-wise manner. First, rates for counties with exactly one missing neighbor are imputed by averaging the available neighboring county rates. Next, counties with two missing neighbors are addressed in the same way, followed by those with three missing neighbors. This process repeats iteratively, cycling through these steps until all counties with at least one missing neighbor are addressed. This leaves only those counties where all neighbors have available data. These counties are handled at the end because they do not impact the earlier steps, and their missing rates are imputed by averaging over the full set of neighboring counties.

Next, we address island counties with missing data. These counties are geographically separated from the mainland and therefore lack queen adjacent neighbors. For these island counties, which number at most three in any given year, we construct neighborhoods using the closest continental neighbors. Missing rates are then imputed by averaging rates over these constructed continental neighborhoods.

Finally, Connecticut’s county structure underwent a complete change in 2022. Since our dataset is curated to reflect the 2022 county boundaries, we needed to account for this structural change in all prior years of the study. To do this, we used the Python package Tobler [48], which specializes in spatial interpolation. Tobler allowed us to transfer data from the old county boundaries (2010 to 2021) to the new 2022 structure by interpolating mortality rates between the two geographic frameworks. This interpolation adjusts for differences in county areas, and ensures that population-dependent variables like mortality rates are accurately represented in the new structure.

To demonstrate the effectiveness of our methodology, we showcase national maps for the year 2013. This year had the most significant data gaps, with 1,681 out of 3,144 counties lacking mortality rate data. Figure 7 displays maps both with and without the missing data, each colored by percentiles from the respective empirical distributions. Figure 7a illustrates the extent of the missing data, revealing an incomplete view of national mortality rates. In contrast, Figure 7b shows the results after applying our imputation method; previously missing regions are now filled with interpolated data that preserves spatial patterns and maintains the integrity of the original dataset. This significant improvement highlights the robustness of our approach, allowing us to address substantial data gaps and create a more complete and accurate national dataset for analysis.

Figure 8 demonstrates the results of using the Tobler library to interpolate mortality rates for Connecticut in 2021, the last year before the county structure changed. Figure 8a displays Connecticut’s old county structure (pre-2022), while Figure 8b shows the new 2022 boundaries. For direct comparison, the color scales for both maps are normalized to the minimum and maximum 2021 mortality rates across both county structures. As an example, counties 09003 and 09013 from the old structure roughly correspond to county 09110 in the new 2022 structure. Here the interpolated data accurately reflects this consolidation, with the interpolated value being substantially larger than both old values. For another example, county 09009 in the old structure roughly corresponds to counties 09140 and 09170 in the new structure. In this example, the interpolated data captures this division effectively, with both interpolated values considerably lower than the old value.

SVI data

This study uses county-level rank ordered percentile estimates (ranging from 0 to 100) of thirteen social vulnerability factors across the United States from 2010 to 2022. The set of SVI variables utilized for 2010 data collection differs from those used in 2022. Therefore, we were forced to exclude all variables that were not available across every year in the study period, resulting in the thirteen SVI variables utilized in this study. All data were sourced from the CDC and the Agency for Toxic Substances and Disease Registry’s Social Vulnerability Index, which utilizes data from the American Community Survey to assess the resilience of communities to external stresses on human health [7].

The 2010 SVI data was not followed by another release until 2014, after which the data has been released biennially. To account for the gap between 2010 and 2014, we imputed the intervening years by calculating a quarter of the difference between the 2010 and 2014 data points and adding it consecutively to each year starting in 2014. After 2014, for the biennial data releases, we applied a similar method by calculating half the difference between consecutive data points and adding it to the earlier year’s rates. This method, with the understanding that yearly rate fluctuations are modest, provided a viable way to analyze the impact of these social vulnerability factors on the

national opioid crisis throughout the entire study period.

Notably, Rio Arriba County, New Mexico, experienced a data collection error in 2018 [49]. Therefore, for this county, we applied the same approach used for the gap between 2010 and 2014, taking a quarter of the difference between the 2016 and 2020 data points and adding it consecutively to each year starting in 2016. Overall, the SVI data had minimal missing values, at most four counties in any given year of the study. These missing rates were imputed using the exact same methodology employed for the mortality rates.

XGBoost model

In this study, XGBoost was used to predict opioid-related mortality rates from 2011 to 2022 based on the previous year’s SVI data. To use XGBoost, several parameters need to be selected, such as the number and depth of trees. To select these parameters, we employed a grid search algorithm with cross-validation, optimizing for the highest predictive accuracy. For training and testing, we used 5-fold cross-validation to randomly split the SVI input data into five folds. In each fold, XGBoost trained on four subsets and predicted on one. This process was repeated across all five folds to generate predictions for every county, ensuring that the model was both trained and tested on the entire SVI dataset.

To describe this model mathematically, fix a year $t \in \{2010, 2011, \dots, 2021\}$ and let $X^{(t)} = [x_{i,j}^{(t)}] \in \mathbb{R}^{3144 \times 13}$ be the matrix of SVI features input to the model in year t . Each row of matrix $X^{(t)}$ corresponds to a county, while each column corresponds to an SVI variable. In particular, let $x_{i,*}^{(t)}$ denote the row vector containing all the SVI feature data for county i , and let $x_{*,j}^{(t)}$ denote the column vector containing all county rates for SVI variable j . Letting $Y^{(t+1)} = (y_i^{(t+1)}) \in \mathbb{R}^{3144}$ be the target vector of mortality rates in year $t+1$, we can define the full dataset $X^{(t)} \times Y^{(t+1)}$ passing through the model to be the set of all counties’ feature vectors together with their corresponding target values:

$$X^{(t)} \times Y^{(t+1)} = \{(x_{i,*}^{(t)}, y_i^{(t+1)}) \mid i \in \{1, 2, \dots, 3144\}\}$$

Starting with the root node, an individual decision tree grows by recursively applying a splitting process to each node n in the tree. Let the data at node n be denoted by Q_n with s_n samples. Then s_n is the number of counties which reached that node, and $Q_n \subseteq X^{(t)} \times Y^{(t+1)}$ is the subset of data for those counties. At each node, a potential split $\theta = (j, h_n)$, consisting of an SVI feature j and a threshold h_n , partition Q_n into two subsets:

$$\begin{aligned} Q_n^{left}(\theta) &= \{(x_{i,*}^{(t)}, y_i^{(t+1)}) \mid x_{i,j}^{(t)} \leq h_n\}, \\ Q_n^{right}(\theta) &= Q_n \setminus Q_n^{left}(\theta). \end{aligned}$$

$Q_n^{left}(\theta)$ is the data for counties satisfying the boolean condition of the split, meaning these data points proceed down the tree's left path; while $Q_n^{right}(\theta)$ contains the data for counties which did not satisfy the split condition, meaning these data points proceed down the right path. The quality of a potential split at node n is measured using a loss function $L(Q)$ which evaluates how well the data in an arbitrary set Q fits the target values. In particular, we utilize the mean absolute error as the loss function:

$$L(Q) = \frac{1}{|Q|} \sum_{(x_{i,*}^{(t)}, y_i^{(t+1)}) \in Q} |y_i^{(t+1)} - \hat{y}_i^{(t+1)}|,$$

where $\hat{y}_i^{(t+1)}$ is the predicted mortality rate for county i .

The gain $G(Q_n, \theta)$ from splitting Q_n by θ is then given by

$$G(Q_n, \theta) = L(Q_n) - \left(\frac{s_n^{left}}{s_n} L(Q_n^{left}(\theta)) + \frac{s_n^{right}}{s_n} L(Q_n^{right}(\theta)) \right). \quad (1)$$

Here s_n^{left} is the number of counties which satisfied the split condition, and s_n^{right} is the number that did not. The optimal split $\tilde{\theta}$ at this node is then chosen by maximizing the gain:

$$\tilde{\theta} = \operatorname{argmax}_{\theta} G(Q_n, \theta). \quad (2)$$

This process creates child nodes from the subsets $Q_n^{left}(\tilde{\theta})$ and $Q_n^{right}(\tilde{\theta})$. It continues recursively until a stopping criterion is met, such as reaching the minimum number of samples at a node or when no further improvement in gain is possible. Mortality rate predictions are then made at these nodes with no further splits, called leaf nodes or terminal nodes. If n is a terminal node, then the prediction for each county i which reached this node is

$$\hat{y}_i^{(t+1)} = \frac{1}{s_n} \sum_{(x_{i,*}^{(t)}, y_i^{(t+1)}) \in Q_n} y_i^{(t+1)}.$$

To evaluate the importance of each SVI feature in the model, XGBoost utilizes the gain from eq. (1). This metric reflects the improvement in the model's predictive performance when an SVI feature is used to split a decision node. At each node, the optimal split was chosen via eq. (2), which can be rewritten as follows:

$$(\tilde{j}, \tilde{h}_n) = \operatorname{argmax}_{j, h_n} G(Q_n, (j, h_n)). \quad (3)$$

From eq. (3), we see that at each node, XGBoost evaluates all features $j \in \{1, 2, \dots, 13\}$ and selects the optimal feature \tilde{j} , along with a corresponding threshold, to maximize the gain.

As the decision trees are built, XGBoost sums the gains for each feature across all nodes and trees in the model. The total gain for feature j , denoted $G_{total}(j)$, is then the sum of the gains $G(Q_n, (\tilde{j}, \tilde{h}_n))$ over all nodes n in the model which split using feature j :

$$G_{total}(j) = \sum_{n=1}^J G(Q_n, (\tilde{j}, \tilde{h}_n)).$$

Here J is the number of nodes which used feature j to split. The features that contribute the most to improving the model’s predictive accuracy are those with the highest total gain. Consequently, features with higher total gain are considered more important, as they most consistently reduce the prediction error across the model.

Autoencoder model

In this study, the autoencoder model was used to predict opioid-related mortality rates from 2011 to 2022 based on the previous year’s SVI data. The input data is first passed through the initial 1D convolutional layer, which aggregates the SVI variables before being fed into the encoder. The encoder compresses the data into a lower-dimensional representation, which is then passed to the decoder to produce the final vector containing yearly mortality rate predictions for each county in the nation.

To preserve the natural temporal structure of the opioid crisis, the model is trained sequentially on SVI data from 2010 to 2020, with 2015 held out as the validation set, and 2021 used for testing. To prevent overfitting, the model is allowed to train for up to 100 epochs, with early stopping triggered after 10 consecutive worse predictions on the validation set. The training process utilizes an L1 loss function and a cyclical learning rate.

To describe the autoencoder model mathematically, again let $t \in \{2010, 2011, \dots, 2021\}$ denote a fixed year, and $X^{(t)}$ denote the input SVI data from year t . Let $\hat{Y}^{(t+1)}$ be the output vector of mortality rate predictions for year $t + 1$, and let A be the full neural network model. It consists of five layers: the initial 1D convolutional layer C , two encoding layers E_1 and E_2 , and two decoding layers D_3 and D_4 . Then the model can be expressed as follows:

$$\begin{aligned} \hat{Y}^{(t+1)} &= A(X^{(t)}) \\ &= (D_4 \circ D_3 \circ E_2 \circ E_1 \circ C)(X^{(t)}). \end{aligned}$$

The convolutional layer C learns an effective way to convolve the thirteen SVI variables, producing a single vector of size 3144. This vector represents the aggregate state of the nation with

respect to the SVI variables. The convolutional layer can be written as:

$$C(X^{(t)}) = W_C \cdot X^{(t)} + b_C,$$

where W_C is the matrix of weights for this layer, and b_C is the vector of biases, both optimized through a stochastic gradient descent process.

The encoder layers E_1 and E_2 iteratively reduce the dimensionality of the input data. E_1 is followed by a ReLU activation function, while E_2 is not. For an arbitrary input x , these layers can be written as follows:

$$\begin{aligned} E_1(x) &= \text{ReLU}(W_{E_1} \cdot x + b_{E_1}), \\ E_2(x) &= W_{E_2} \cdot x + b_{E_2}. \end{aligned}$$

Here W_{E_i} and b_{E_i} are the weight matrices and bias vectors for $i \in \{1, 2\}$, respectively.

The decoder layers D_3 and D_4 then iteratively increase the dimensionality back to the original input space. For an arbitrary input x , these layers can be written as follows:

$$\begin{aligned} D_3(x) &= \text{ReLU}(W_{D_3} \cdot x + b_{D_3}) \\ D_4(x) &= W_{D_4} \cdot x + b_{D_4}. \end{aligned}$$

Here W_{D_i} and b_{D_i} are the weight matrices and bias vectors for $i \in \{3, 4\}$, respectively.

To gain insight into the most important features in the autoencoder’s mortality predictions, we employed a Shapley gradient explainer. This method, building on the concept of integrated gradients [50], utilizes the expected gradient approach to quantify the impact of each input feature [51]. Expected gradients are calculated by averaging the gradient of the model’s output with respect to each feature over the entire county structure, providing a measure of how each feature impacts the autoencoder’s predictions. Each feature’s impact is quantified via a SHAP value, representing the contribution of that feature to the predicted mortality rates. Consequently, the most important features in the autoencoder model are those for which minor perturbations produce the greatest changes in the model’s output.

Acknowledgments

Future acknowledgments here.

Funding

This work is sponsored by the US Department of Veterans Affairs using resources from the Knowledge Discovery Infrastructure which is located at the Oak Ridge National Laboratory and supported by the Office of Science of the U.S. Department of Energy. This manuscript has been authored by UT-Battelle, LLC, under contract DE-AC05-00OR22725 with the US Department of Energy (DOE). The US government retains and the publisher, by accepting the article for publication, acknowledges that the US government retains a nonexclusive, paid-up, irrevocable, worldwide license to publish or reproduce the published form of this manuscript, or allow others to do so, for US government purposes. DOE will provide public access to these results of federally sponsored research in accordance with the DOE Public Access Plan (<http://energy.gov/downloads/doe-public-access-plan>)

Author contributions

AD conducted all core research activities, curated and analyzed the data, generated the code, and wrote the original manuscript. AS and VM supervised the research while providing general and methodological expertise. DM suggested the use of Tobler for interpolating data in Connecticut. All authors reviewed the manuscript and contributed to revisions.

Data availability

All datasets and code supporting this study are available in the ‘A-Deas/Opioid-Feature-Importance’ Github repository: <https://github.com/A-Deas/Opioid-Feature-Importance>.

References

- [1] CDC Overdose Prevention. Understanding the opioid overdose epidemic. <https://www.cdc.gov/overdose-prevention/about/understanding-the-opioid-overdose-epidemic.html>. Accessed August 1, 2024.
- [2] American Medical Association. Report shows decreases in opioid prescribing, increase in overdoses. <https://www.ama-assn.org/press-center/press-releases/report-shows-decreases-opioid-prescribing-increase-overdoses>. Accessed August 1, 2024.
- [3] National Institute on Drug Abuse. Prescription opioids and heroin research report. <https://nida.nih.gov/publications/research-reports/prescription-opioids-heroin/increased-drug-availability-associated-increased-use-overdose>. Accessed August 1, 2024.

- [4] Lucas Böttcher, Tom Chou, and Maria R. D’Orsogna. Forecasting drug-overdose mortality by age in the united states at the national and county levels. *PNAS Nexus*, 3(2):pgae050, 2024.
- [5] State Health Access Data Assistance Center. The opioid epidemic in the united states. <https://www.shadac.org/opioid-epidemic-united-states>. Accessed September 20, 2024.
- [6] National Academies of Sciences, Engineering, and Medicine, Jonathan K. Phillips, Morgan A. Ford, and Richard J. Bonnie. *Pain Management and the Opioid Epidemic: Balancing Societal and Individual Benefits and Risks of Prescription Opioid Use*. National Academies Press (US), Washington, DC, 2017. Available from: <https://www.ncbi.nlm.nih.gov/books/NBK458661/>.
- [7] Centers for Disease Control and Prevention/Agency for Toxic Substances and Disease Registry. Cdc/atsdr svi data and documentation download. https://www.atsdr.cdc.gov/placeandhealth/svi/data_documentation_download.html. Accessed October 13, 2023.
- [8] Rebecca W. Knoebel and Seong J. Kim. Impact of covid-19 pandemic, social vulnerability, and opioid overdoses in chicago. *AJPM Focus*, 2(2):100086, Jun 2023.
- [9] Patrick J. Joudrey, Marynia Kolak, Qian Lin, Sara Paykin, Vanessa Anguiano, and Emily A. Wang. Assessment of community-level vulnerability and access to medications for opioid use disorder. *JAMA Network Open*, 5(4):e227028, 2022.
- [10] M Tatar, MR Faraji, K Keyes, FA Wilson, and MS Jalali. Social vulnerability predictors of drug poisoning mortality: A machine learning analysis in the united states. *Am J Addict*, 32(6):539–546, 2023.
- [11] T.C. Yang, S. Kim, S.A. Matthews, and C. Shoff. Social vulnerability and the prevalence of opioid use disorder among older medicare beneficiaries in u.s. counties. *Journal of Gerontology: Series B*, 78(12):2111–2121, December 2023.
- [12] Centers for Disease Control and Prevention. Cdc wonder. <https://wonder.cdc.gov/>, 2024. Accessed August 1, 2024.
- [13] Tianqi Chen and Carlos Guestrin. Xgboost: A scalable tree boosting system. In *Proceedings of the 22nd ACM SIGKDD International Conference on Knowledge Discovery and Data Mining*, volume 11 of *KDD ’16*, page 785–794. ACM, August 2016.
- [14] Dwi Tarwidi, Sri R. Pudjaprasetya, Donny Adytia, and Muwafiq Apri. An optimized xgboost-based machine learning method for predicting wave run-up on a sloping beach. *MethodsX*, 10:102119, Mar 10 2023.

- [15] Kartik Budholiya, Shailendra Kumar Shrivastava, and Vivek Sharma. An optimized xgboost based diagnostic system for effective prediction of heart disease. *Journal of King Saud University - Computer and Information Sciences*, 34(7):4514–4523, 2022.
- [16] Andrew Moore and Melanie Bell. Xgboost, a novel explainable ai technique, in the prediction of myocardial infarction: A uk biobank cohort study. *Clinical Medicine Insights: Cardiology*, 16:11795468221133611, Nov 8 2022.
- [17] Dor Bank, Noam Koenigstein, and Raja Giryes. Autoencoders, 2021.
- [18] Pengzhi Li, Yan Pei, and Jianqiang Li. A comprehensive survey on design and application of autoencoder in deep learning. *Applied Soft Computing*, 138:110176, 2023.
- [19] Kamran Berahmand, Farhad Daneshfar, Ehsan S. Salehi, and et al. Autoencoders and their applications in machine learning: a survey. *Artificial Intelligence Review*, 57(28), 2024.
- [20] Scott Lundberg. shap.gradientexplainer. <https://shap.readthedocs.io/en/latest/generated/shap.GradientExplainer.html>, 2018. Accessed July 15, 2024.
- [21] Scott M. Lundberg and Su-In Lee. A unified approach to interpreting model predictions. In *Proceedings of the 31st International Conference on Neural Information Processing Systems*, NIPS’17, page 4768–4777, Red Hook, NY, USA, 2017. Curran Associates Inc.
- [22] Alex Hollingsworth, Christopher J. Ruhm, and Kosali Simon. Macroeconomic conditions and opioid abuse. Working Paper 23192, National Bureau of Economic Research, Feb 2017.
- [23] UCLA Nursing. Opioid addiction crisis in united states linked to poor working conditions and unemployment. <https://nursing.ucla.edu/news/opioid-addiction-crisis-in-united-states-linked-to-poor>, 2022. Accessed September 17, 2024.
- [24] August F. Holtyn, Fabian Toegel, Michael D. Novak, and Kenneth Silverman. Factors associated with obtaining employment among opioid use disorder patients enrolled in a therapeutic workplace intervention. *Drug and Alcohol Dependence*, 226:108907, Sep 1 2021.
- [25] Timothy A. Matthews, Grace Sembajwe, Roland von Känel, and Jian Li. Associations of employment status with opioid misuse: Evidence from a nationally representative survey in the u.s. *Journal of Psychiatric Research*, 151:30–33, 2022.
- [26] Sunday Azagba, Ling Shan, Fares Qeadan, and et al. Unemployment rate, opioids misuse and other substance abuse: quasi-experimental evidence from treatment admissions data. *BMC Psychiatry*, 21(22), 2021.

- [27] ASPE Office of the Assistant Secretary for Planning and Evaluation. Economic opportunity and the opioid crisis: Geographic and economic trends. <https://aspe.hhs.gov/reports/economic-opportunity-opioid-crisis-geographic-economic-trends>. Accessed September 17, 2024.
- [28] Mercy N. Mumba, Lori Davis, Nancy L. Smith, Tiffany Evans, and Ruben Castillo. Effects of unemployment on opioid use treatment trajectories: Impact of the covid-19 pandemic. *Journal of Addictions Nursing*, 33(3):168–171, Jul-Sep 2022.
- [29] M. Kate Wolfe, Noreen C. McDonald, and George M. Holmes. Transportation barriers to health care in the united states: Findings from the national health interview survey, 1997-2017. *American Journal of Public Health*, 110(6):815–822, Jun 2020.
- [30] Samina T. Syed, Benjamin S. Gerber, and Lisa K. Sharp. Traveling towards disease: transportation barriers to health care access. *Journal of Community Health*, 38(5):976–993, Oct 2013.
- [31] Robert Wood Johnson Foundation. More than one in five adults with limited public transit access forgo health care because of transportation barriers. <https://www.rwjf.org/en/insights/our-research/2023/04/more-than-one-in-five-adults-with-limited-public-transit-access-forgo-healthcare-because-of-transportation-barriers.html>. Accessed September 17, 2024.
- [32] CM Nguyen, G Kubiak, N Dixit, SA Young, and JR Hayes. Evaluating barriers to opioid use disorder treatment from patients’ perspectives. *PRiMER*, 8:11, 2024.
- [33] American Hospital Association. Social determinants of health series: Transportation and the role of hospitals. <https://www.aha.org/ahahret-guides/2017-11-15-social-determinants-health-series-transportation-and-role-hospitals#:~:text=Transportation%20issues%20can%20affect%20a,be%20a%20vehicle%20for%20wellness>. Accessed September 17, 2024.
- [34] Marwan Labban, Chia-Yuan Chen, Natalie Frego, and et al. Disparities in travel-related barriers to accessing health care from the 2017 national household travel survey. *JAMA Network Open*, 6(7):e2325291, 2023.
- [35] Marjorie C. Gondré-Lewis, Tomilola Abijo, and Theodore A. Gondré-Lewis. The opioid epidemic: a crisis disproportionately impacting black americans and urban communities. *Journal of Racial and Ethnic Health Disparities*, 10(4):2039–2053, Aug 2023.

- [36] RW Knoebel and SJ Kim. Impact of covid-19 pandemic, social vulnerability, and opioid overdoses in chicago. *AJPM Focus*, 2(2):100086, 2023.
- [37] Erin J. Stringfellow, Tse Yang Lim, Catherine DiGennaro, Zeynep Hasgul, and Mohammad S. Jalali. Enumerating contributions of fentanyl and other factors to the unprecedented 2020 rise in opioid overdose deaths: model-based analysis. *PNAS Nexus*, 2(4):pgad064, 2023.
- [38] Allison L. Cochran, Noreen C. McDonald, Laura Prunkl, and et al. Transportation barriers to care among frequent health care users during the covid pandemic. *BMC Public Health*, 22(1783), 2022.
- [39] Nicholas Morrish and Antonia Medina-Lara. Does unemployment lead to greater levels of loneliness? a systematic review. *Social Science & Medicine*, 287:114339, Oct 2021.
- [40] Francesco Bianchi, Giada Bianchi, and Dongho Song. The long-term impact of the covid-19 unemployment shock on life expectancy and mortality rates. *Journal of Economic Dynamics and Control*, 146:104581, 2023.
- [41] Alicia Jeffers, Alisha A. Meehan, Joseph Barker, Alyson Asher, Misty P. Montgomery, Gabriella Bautista, Catherine M. Ray, Richard L. Laws, Vanessa L. Fields, Lakshmi Radhakrishnan, Seong Y. Cha, Ann Christensen, Brisnedy Dupervil, Jessica V. Verlenden, Christie H. Cassell, Anne Boyer, Beth DiPietro, Mary Cary, Miwa Yang, Emily Mosites, and Rachel Marcus. Impact of social isolation during the covid-19 pandemic on mental health, substance use, and homelessness: Qualitative interviews with behavioral health providers. *International Journal of Environmental Research and Public Health*, 19(19):12120, Sep 25 2022.
- [42] Congressional Research Service. Unemployment rates during the covid-19 pandemic. Technical report, Congressional Research Service, 2021. Accessed August 1, 2024.
- [43] United States Census Bureau. Table & geography changes. <https://www.census.gov/programs-surveys/acs/technical-documentation/table-and-geography-changes.2022.html#list-tab-71983198>. Accessed October 19, 2023.
- [44] Federal Register. Change to county-equivalents in the state of connecticut. <https://www.federalregister.gov/documents/2022/06/06/2022-12063/change-to-county-equivalents-in-the-state-of-connecticut>. Accessed September 1, 2024.
- [45] CDC National Center for Health Statistics. Icd-10. https://www.cdc.gov/nchs/icd/icd-10/index.html#cdc_generic_section.3-icd-10, 2024. Accessed August 1, 2023.

- [46] CDC National Center for Health Statistics. Provisional drug overdose death counts. <https://www.cdc.gov/nchs/nvss/vsrr/drug-overdose-data.htm>, 2024. Accessed August 1, 2023.
- [47] Chandra Tiwari, Kirsten Beyer, and Gerard Rushton. The impact of data suppression on local mortality rates: the case of cdc wonder. *American Journal of Public Health*, 104(8):1386–1388, Aug 2014.
- [48] PySAL Development Team. Tobler github repository. <https://github.com/pysal/tobler>, 2023. Accessed August 30, 2024.
- [49] United States Census Bureau. Data collection error in rio arriba county, nm. <https://www.census.gov/programs-surveys/acs/technical-documentation/errata/125.html>. Accessed February 15, 2024.
- [50] Mukund Sundararajan, Ankur Taly, and Qiqi Yan. Axiomatic attribution for deep networks. In *Proceedings of the 34th International Conference on Machine Learning - Volume 70, ICML'17*, page 3319–3328. JMLR.org, 2017.
- [51] G Erion, JD Janizek, P Sturmfels, S Lundberg, and SI Lee. Improving performance of deep learning models with axiomatic attribution priors and expected gradients, 2020.

Figures and Tables

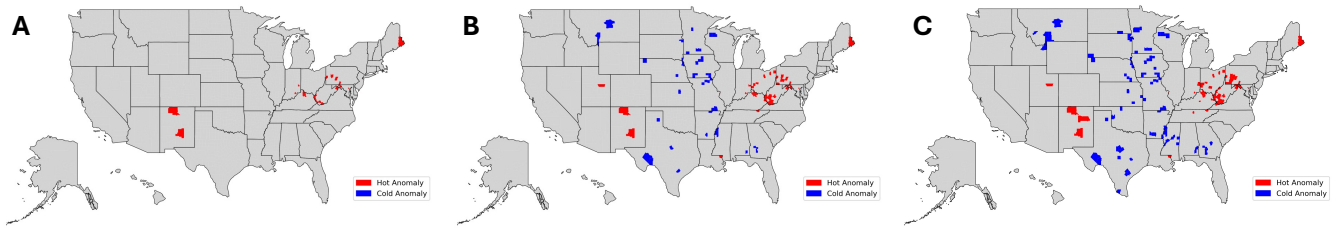


Figure 1: A) 2016 anomaly map using 1% tails. B) 2016 anomaly map using 2% tails. C) 2016 anomaly map using 3% tails. A 1% threshold produced no cold anomalies. A 2% threshold was the tightest bound that yielded cold anomalies. A 3% threshold increased the number of anomalies.

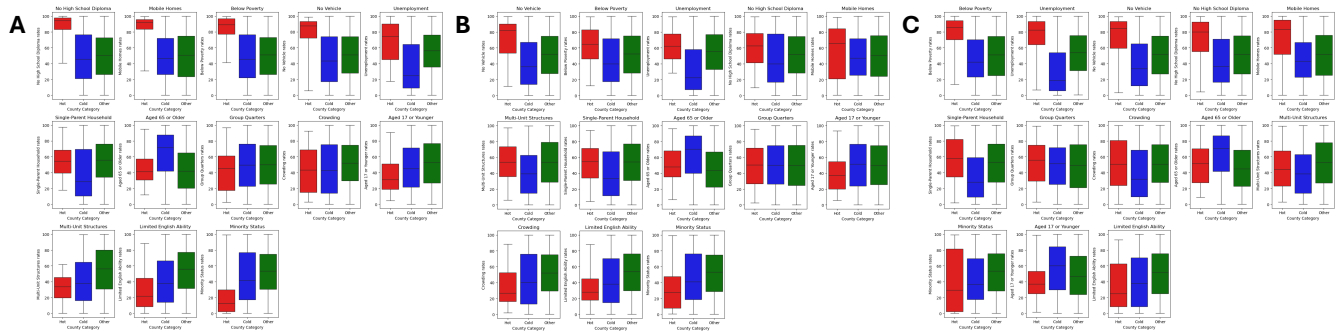


Figure 2: A) 2010 boxplots. B) 2016 boxplots. C) 2022 boxplots. The boxplots visualize the national distribution of each SVI variable’s rates. Variables are arranged from top left to bottom right, beginning with the highest average rate in the hot counties and ending with the lowest.

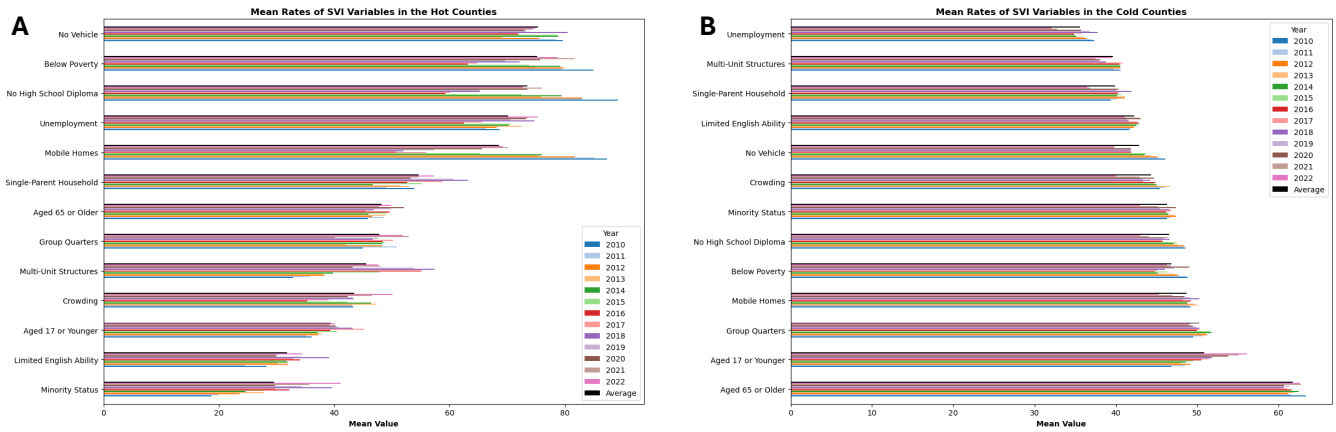


Figure 3: A) Hot anomaly summary. B) Cold anomaly summary. In both plots, each feature’s yearly mean rates are displayed using colored bars, while the black bars showcase each feature’s average mean rate across all years in the study. In the hot anomaly summary, features are ranked from highest average mean rate down to lowest. In the cold anomaly summary, features are ranked from lowest average mean rate down to highest. Figures are best viewed in color.

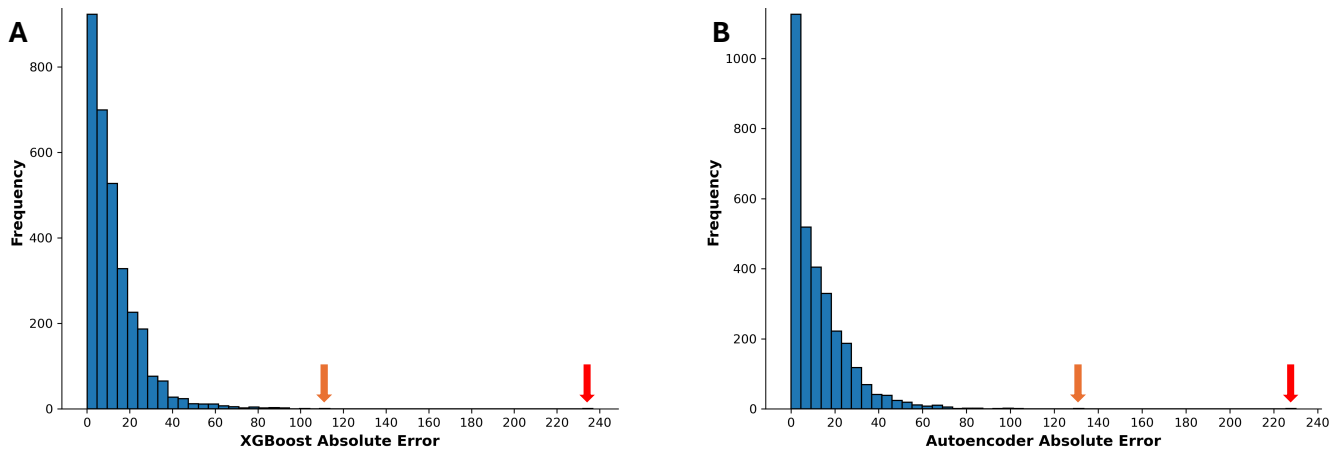


Figure 4: A) Histogram displaying the distribution of XGBoost’s absolute errors for the 2022 mortality rate predictions. B) Histogram displaying the distribution of the autoencoder’s absolute errors for the 2022 mortality rate predictions. In both plots, the error stemming from Menominee County, Wisconsin, is indicated by the red arrow, while the error stemming from Bath County, Kentucky, is indicated by the orange arrow.

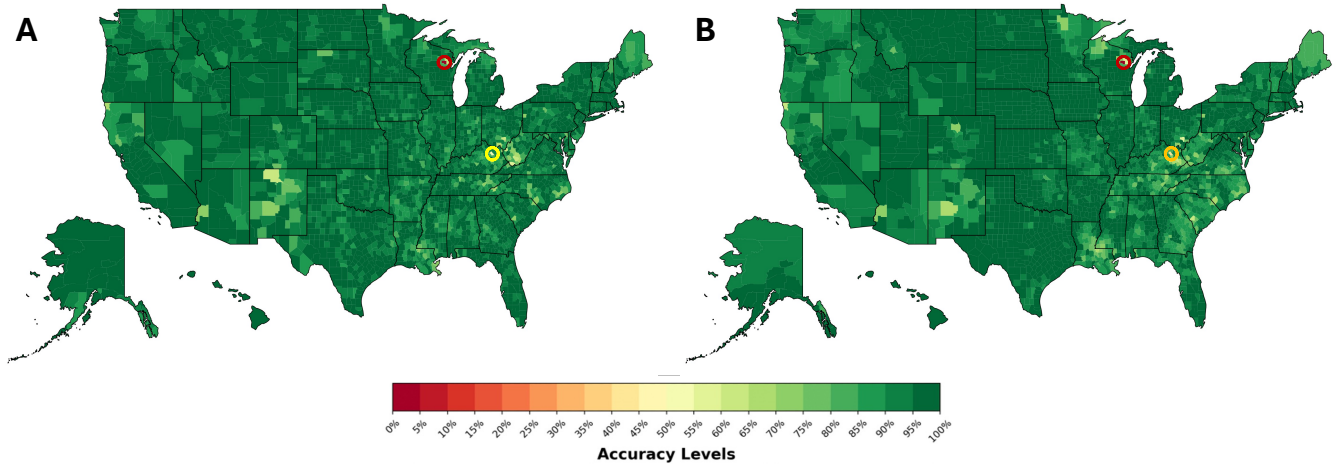


Figure 5: A) Accuracy map for XGBoost’s 2022 mortality rate predictions. B) Accuracy map for the autoencoder’s 2022 mortality rate predictions. Both maps are color-coded to represent increasing intervals of accuracy by 5%, starting from dark red for the least accurate predictions, and progressing to dark green for the most accurate predictions. In both plots, Menominee County, Wisconsin, which had the largest 2022 error for both models, is shaded in the darkest red. To make it easier to locate, this county is also circled in the same color. Bath County, Kentucky, is shaded in orange on the autoencoder’s accuracy map and in yellow on XGBoost’s map, highlighting that the autoencoder had a higher error here than XGBoost. This county has also been circled in its respective color for easier visual identification. Figures are best viewed in color.

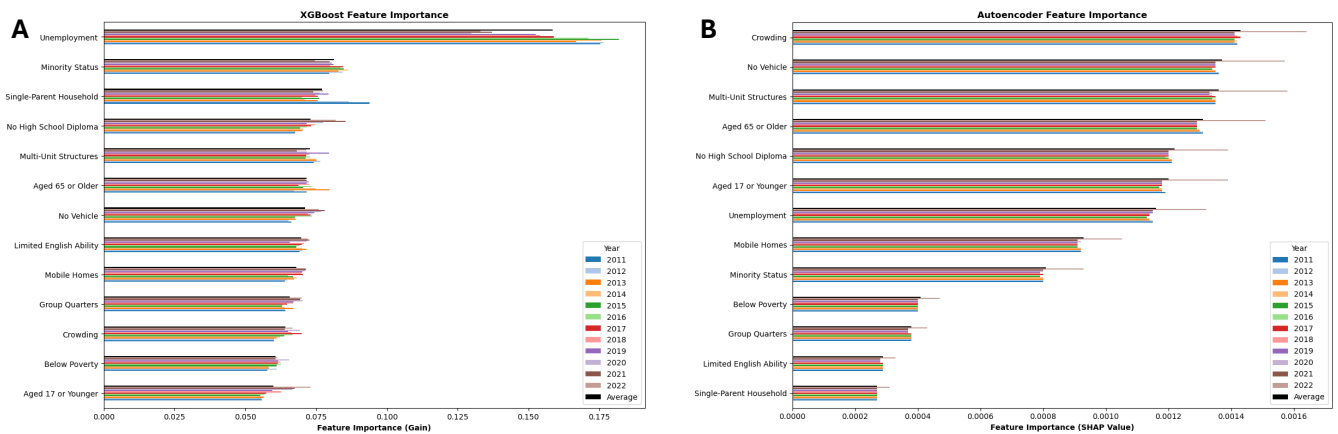


Figure 6: A) XGBoost feature importance summary. B) Autoencoder feature importance summary. In both plots, each feature’s yearly importance scores are displayed using colored bars, while the black bars showcase each feature’s average importance scores across all years in the study. Features are ranked from highest average importance down to lowest. Figures are best viewed in color.

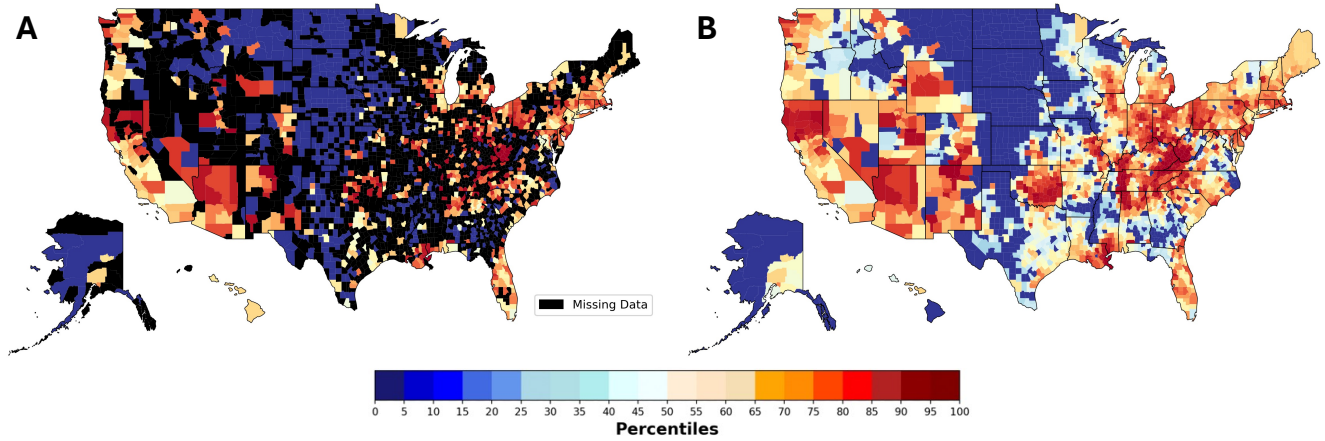


Figure 7: A) 2013 missing data map. B) 2013 interpolated data map. Each map is colored by percentiles from the respective empirical distributions.

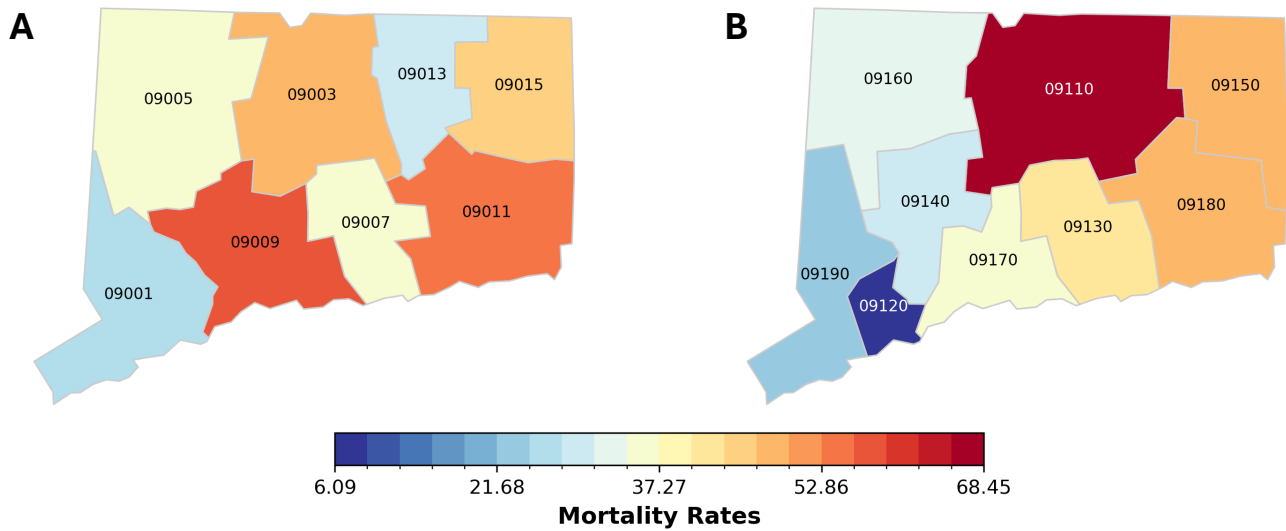


Figure 8: A) 2021 mortality rates for the old (pre-2022) Connecticut county structure. B) 2021 mortality rates for the new (2022) Connecticut county structure. The color scales for both maps are normalized to the minimum and maximum 2021 mortality rates across both county structures. The minimum 2021 mortality rate is 6.09, shown in the darkest blue, while the maximum rate is 68.45, shown in the darkest red.

Theme	Feature	Definition
Socioeconomic Status	Below poverty	Percentile percentage of persons below poverty estimate
	Unemployment	Percentile percentage of civilian (age 16+) unemployed estimate
	No high school diploma	Percentile percentage of persons with no high school diploma (age 25+) estimate
Household Characteristics	Age 65 and older	Percentile percentage of persons aged 65 and older estimate
	Age 17 and younger	Percentile percentage of persons aged 17 and younger estimate
	Single-parent households	Percentile percentage of single-parent households with children under 18 estimate
	Limited English ability	Percentile percentage of persons (age 5+) who speak English “less than well” estimate
Racial and Ethnic Minority Status	Minority Status	Percentile percentage minority (Hispanic or Latino (of any race); Black and African American, Not Hispanic or Latino; American Indian and Alaska Native, Not Hispanic or Latino; Asian, Not Hispanic or Latino; Native Hawaiian and Other Pacific Islander, Not Hispanic or Latino; Two or More Races, Not Hispanic or Latino; Other Races, Not Hispanic or Latino) estimate
Housing Type and Transportation	Multi-unit structures	Percentile percentage of housing structures with 10 or more units estimate
	Mobile homes	Percentile percentage mobile homes estimate
	Crowding	Percentile percentage of households with more people than rooms estimate
	No vehicle	Percentile percentage of households with no vehicle available estimate
	Group quarters	Percentile percentage of persons in group quarters estimate (e.g., correctional institutions, nursing homes)

Table 1: Definitions of the social vulnerability features utilized in this study.

Year	Avg Error		Max Error		Avg Accuracy	
	XGB	AE	XGB	AE	XGB	AE
2011	5.79	4.07	100.18	72.41	94.22%	94.39%
2012	5.67	4.08	72.14	72.88	92.14%	94.40%
2013	5.86	3.97	78.39	55.25	92.52%	92.82%
2014	6.43	3.56	87.57	59.17	92.66%	93.98%
2015	6.65	3.26	112.40	68.05	94.09%	95.22%
2016	7.83	4.66	107.68	100.36	92.73%	95.36%
2017	8.34	4.15	126.24	72.20	93.39%	94.25%
2018	8.18	3.94	98.80	48.67	91.72%	91.91%
2019	8.43	4.02	97.56	60.61	91.36%	93.36%
2020	10.78	7.35	136.70	92.04	92.11%	92.02%
2021	13.84	11.60	161.62	184.12	92.06%	93.70%
2022	12.44	12.37	236.83	230.10	94.75%	94.62%

Table 2: Efficacy metric summary for both the XGBoost (XGB) and autoencoder (AE) models. For each county, the error is measured as the absolute residual, while the accuracy is calculated as the county’s error normalized by the highest observed error nationwide.